Design and Synthesis of Polymer-Functionalized NIR Fluorescent Dyes—Magnetic Nanoparticles for Bioimaging

Swee Kuan Yen,[†] Dominik Jańczewski,[†] Jeeva Lavanya Lakshmi,[†,‡] Surani Bin Dolmanan,[†] Sudhiranjan Tripathy,[†] Vincent H. B. Ho,[§] Vimalan Vijayaragavan,[⊥] Anushya Hariharan,[⊥,#] Parasuraman Padmanabhan,[⊥,∥] Kishore K. Bhakoo,[⊥] Thankiah Sudhaharan,[#] Sohail Ahmed,[#] Yong Zhang,[‡] and Subramanian Tamil Selvan[†,‡,*]

[†]Institute of Materials Research and Engineering (IMRE), A*STAR (Agency for Science, Technology and Research), 3 Research Link, Singapore 117602, [‡]Department of Bioengineering, Faculty of Engineering, National University of Singapore, 7 Engineering Drive 1 Singapore 117576, [§]Molecular Engineering Laboratory, A*STAR, 61 Biopolis Drive, #03-13 Proteos, Singapore 138673, [⊥]Singapore Bioimaging Consortium (SBIC), A*STAR, 11 Biopolis Way, #02-02 Helios, Singapore 138667, and [#]Institute of Medical Biology (IMB), A*STAR, 8A Biomedical Grove, Immunos, Singapore 138648. [∥]Present address: The Lee Kong Chian School of Medicine, Nanyang Technological University, 50 Nanyang Drive, Research Techno Plaza, Level 4, X-Frontier Block, Singapore 637553.

ABSTRACT The fluorescent probes having complete spectral separation between absorption and emission spectra (large Stokes shift) are highly useful for solar concentrators and bioimaging. In bioimaging application, NIR fluorescent dyes have a greater advantage in tissue penetration depth compared to visible-emitting organic dyes or inorganic quantum dots. Here we report the design, synthesis, and characterization of an amphiphilic polymer, poly-(isobutylene-*alt*-maleic anhyride)-functionalized near-infrared (NIR) IR-820 dye and its conjugates with iron oxide (Fe_3O_4) magnetic nanoparticles (MNPs) for optical and magnetic resonance (MR) imaging. Our results demonstrate that the Stokes shift of unmodified dye can be tuned (from ~106 to 208 nm) by the functionalization of the dye with polymer and MNPs. The fabrication of bimodal probes involves (i) the synthesis of NIR fluorescent dye (IR-820 cyanine) functionalized with ethylenediamine linker in high yield, >90%, (ii) polymer conjugation to the functionalized NIR fluorescent dye, and (iii) grafting the polymer-conjugated dyes on iron oxide MNPs. The resulting uniform, small-sized (*ca.* 6 nm) NIR fluorescent dye—magnetic hybrid nanoparticles (NPs) exhibit a wider emissive range (800—1000 nm) and minimal cytotoxicity. Our preliminary studies demonstrate the potential utility of these NPs in bioimaging by means of direct labeling of cancerous HeLa cells *via* NIR fluorescence microscopy and good negative contrast enhancement in T_2-weighted MR imaging of a murine model.

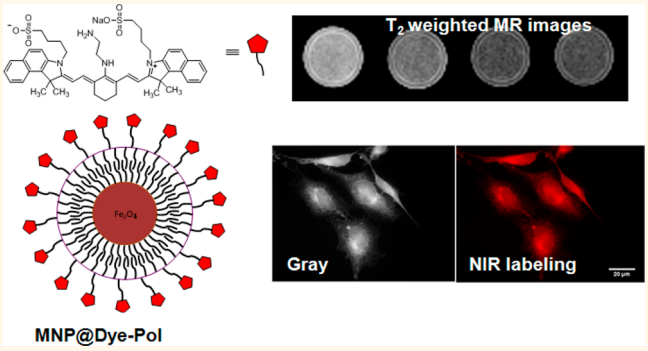

KEYWORDS: near-infrared fluorescent dyes · magnetic nanoparticles · bimodal probes · optical imaging · magnetic resonance imaging

Magnetic nanoparticles (MNPs) have been actively explored as core nanoparticles (NPs) for the fabrication of metal or semiconducting quantum dots as shell NPs and also for appropriate surface conjugation with biomolecules, fluorochromes, and radionuclides for a wide range of biomedical applications.[1−5] The uniform size (<20 nm), narrow particle size distribution, regular shape, high magnetization values, biocompatibility, and nontoxicity make the MNPs ideal candidates for cancer imaging and therapy.[6,7] One of the interesting approaches to combine MRI agents with optical probes is to link MNPs (*e.g.*, iron oxide) with fluorescent quantum dots (QDs).[8−10] Although CdSe/ZnS QDs are more stable in live cells,[11,12] the carcinogenic heavy cadmium metal poses a threat to the *in vivo* imaging of large animals and humans. This warrants an active search for alternative optical probes. The development of an MNP conjugate with an NIR organic dye is such an alternative.

NIR organic dyes provide unique absorption bands in the wavelength range

* Address correspondence to subramaniant@imre.a-star.edu.sg; biests@nus.edu.sg.

Received for review April 9, 2013 and accepted July 19, 2013.

Published online July 19, 2013
10.1021/nn401734t

600−1000 nm.[13] It is referred to as the "NIR optical window" that is ideally suited for *in vivo* imaging of cells and tissues, where NIR light is poorly absorbed, resulting in deep tissue penetration and negligible background autofluorescence.[14] A major impact for imaging tumors *in vivo* has resulted from some of the recent developments of NIR fluorochromes[15−20] and type II QDs.[21] Highly sensitive NIR optical probes were also designed for the sensing of nitric,[22] zinc,[23,24] and mercuric oxides.[25]

There are a limited number of optical reagents available for clinical application, with only indocyanine green (ICG) being approved by the Food and Drug Administration (FDA) for use in humans studies, due to its low toxicity profile.[14,26] However, the heptamethine group of ICG has limited utility for additional functionalization.[13] One of the strategies to overcome this limitation, is to use the heptamethine cyanine dyes with a cyclohexenyl ring for further functionalization, improving solubility and photostability. Therefore, the functionalization of NIR cyanine dyes is highly desirable as probes for imaging applications. Furthermore, the coupling of NIR dye to a polymer or particle can be achieved by the introduction of a suitable functional group with or without linker.[27−31]

Due to the fragile structure of NIR dyes, the chemical modification is not straightforward. A series of diverse *meso*-aminophenyl-, hydroxyphenyl-, and phenyl-substituted heptamethine cyanine dyes were synthesized by a modified Suzuki−Miyaura C−C coupling reaction in one pot, without further conjugation to biomolecules or nanomaterials.[32] Tricarbocyanine-based ratiometric NIR fluorescent probes were synthesized, and their spectral properties designed for esterase and pH stability.[33] There is another example where two heptamethine cyanine dyes were functionalized with alkyl amino groups at the central position.[34] Some of amino-cyanine dyes containing terminal functional groups (acids, azides, and cyclooctyne for further functionalization) were also reported in the group of Weck.[35] The above compounds have not been much applied as optical imaging agents and none of them as bimodal imaging agents. An NIR indocyanine dye conjugate with an organic polyamine polymer (polyethylenimine) with a less hindered carboxy-terminal amino linker was also synthesized.[36,37] This conjugate was able to bind to DNA and could be monitored *in vivo* using noninvasive optical imaging. Although the above reports focused on the synthesis of NIR dyes, the product yields were relatively lower.

In the context of bimodal imaging involving optical probes combined with MRI, there are only a few examples in the literature using MNP conjugates with dyes emitting below <800 nm. Peptides were attached to cross-linked iron oxide (CLIO) NPs *via* a disulfide or thioether linker, followed by the indocyanine dye conjugation,[38] and used as preoperative MRI and intraoperative optical probes.[39] Such bimodal probes with peptide-conjugated Cy5.5-CLIO NPs were designed for *in vivo* targeting of underglycosylated MUC-1 tumor antigen.[40] There are other Cy5.5-CLIO NPs bimodal probes reported for different targeted applications such as annexin V-CLIO-Cy5.5 for binding apoptotic Jurkat T cells,[41] peptide-coated NPs for detection of vascular adhesion molecule-1 expression,[42] NP-Cy5.5 consisting of poly(ethylene glycol) polymer, chlorotoxin, and Cy5.5 for targeting of gliomas,[43] An_xCLIO-Cy5.5 for cardiomyocyte apoptosis,[44] linear RGD-CLIO (Cy5.5) and scrambled RGD-CLIO (Cy5.5) (RGD: cyclic arginine-glycine-aspartic acid) for targeting of integrins on BT-20 tumor,[45] CLIO-Cy5.5 for brain tumor visualization,[46] iron oxide NP-loaded Cy5.5-conjugated oleyl-chitosan for detection of tumor *in vivo*,[47] and iron oxide NPs coated with PEG-CTX-Cy5.5 (CTX: chlorotoxin) for specific accumulation in xenograft tumors of a brain tumor model.[48]

In this report, we demonstrate a well-defined synthesis of water-soluble NIR fluorescent dye−magnetic probes for MR and optical imaging applications. A novel tailor-designed synthesis of polymer-functionalized NIR fluorescent dyes emitting above 800 nm, combined with iron oxide MNPs, is presented. The preliminary *in vivo* MR imaging and NIR optical labeling studies clearly demonstrate the practical application of these bimodal probes in the area of multimodal imaging.

RESULTS AND DISCUSSION

Synthesis of IR-820 dye-NH_2, Dye-Pol, and MNP@Dye-Pol. To fabricate a suitable polymeric coating for the iron oxide MNPs, IR-820 cyanine dye was chosen due to its structural similarity to ICG[14] and IR Dye78 (polysulfonated indocyanines) and related lower toxicity.[49] The heterocyclic nitrogen rings provide the fluorescence, and the alkyl-sulfonate groups contribute to the water solubility. Chemical modification without a catalyst was carried out on the central *meso*-chloro cyclohexenyl group of NIR heptamethine cyanine IR-820. In an effort to develop an improved synthetic method of IR-820 for further conjugation, *meso*-halogen was substituted by ethylenediamine in the presence of BuLi at low temperature to avoid decomposition of the dye (Scheme 1). The formation of ethylenediamine anion created the platform for replacing the *meso*-chlorine in the cyclohexenyl group. The column chromatography of the reaction mixture−filtrate afforded IR-820 dye-NH_2 as a glossy green solid with a yield of 91%. The terminal amine group can be attached to a linker that allows for further functionalization with macromolecules.

Subsequently, the conjugation of IR-820 dye-NH_2 with the polymer was carried out. To create macromolecular-based coating,[50,51] polymeric anhydride was conjugated with IR-820 dye-NH_2 and *n*-octyl amine. As reported earlier,[52−54] the hydrophobic character derived from long aliphatic octylamine groups at the

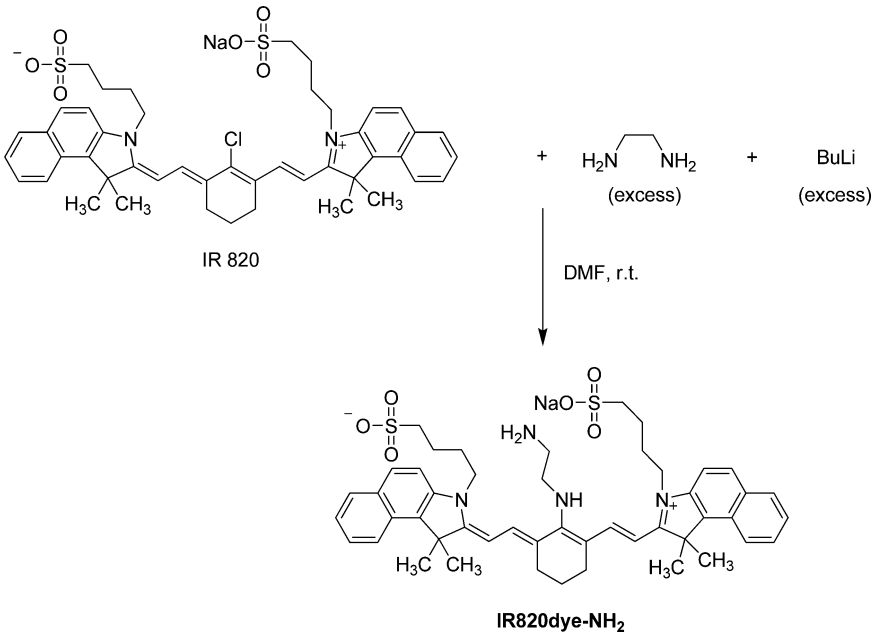

Scheme 1. New designed structure. Reaction replacing the *meso*-chlorine atom of heptamethine cyanine dyes with ethylenediamine, producing an amine-functionalized moiety, IR-820 dye-NH_2.

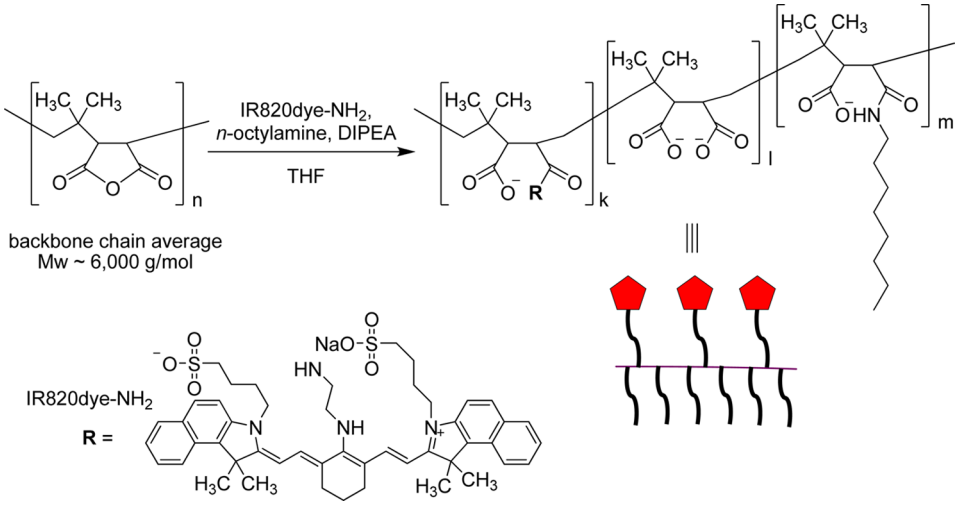

Scheme 2. Scheme depicting the synthesis of dye–polymer conjugate (Dye-Pol), which involves the reaction between the polymer, poly(isobutylene-*alt*-maleic anhydride), and IR-820 dye-NH_2 in the presence of *n*-octylamine and DIPEA in THF.

polymer backbone is responsible for interaction with hydrophobic ligands present on the surface of the MNPs, while carboxylic groups provide colloidal stability in water. In this study, poly(isobutylene-*alt*-maleic anhydride) with a molecular weight (M_w) of 6000 was chosen for conjugation, affording Dye-Pol (Scheme 2). The magnetite (Fe_3O_4) MNPs were synthesized according to a literature procedure with slight modifications.[55] The as-synthesized MNPs were coated with oleylamine, rendering the hydrophobic particle surface. Hydrophobic MNPs were transferred into water using the polymer–dye conjugate (Dye-Pol), following the previously established protocols.[50–54] In this process, the macromolecules were wrapped around the MNPs, resulting in stable, water-soluble assemblies with Dye-Pol (Figure 1a). The water-dispersible NPs (MNP@Dye-Pol) obtained in this way were used for further studies.

Characterization of IR-820 dye-NH_2, Dye-Pol, and MNP@Dye-Pol. The functionalized NIR fluorescent dye, IR-820 dye-NH_2, retained all the traits of NIR dyes such as good water solubility and photochemical properties (at least 2 months of shelf life in refrigerator). The ^{1}H NMR spectrum of IR-820 dye-NH_2 recorded in DMSO-d_6 was similar to that of IR-820 with the extra signals of multiple resonances at 3.42 and 4.35 ppm, characteristic of the aliphatic ethylene substituent. This was further supported by the ^{13}C signal for the formation of IR-820 dye-NH_2 (see Supporting Information). The FTIR spectrum showed the N–H stretching (3500–3100 cm^{-1}) and N–H bending (1550–1450 cm^{-1}) modes.

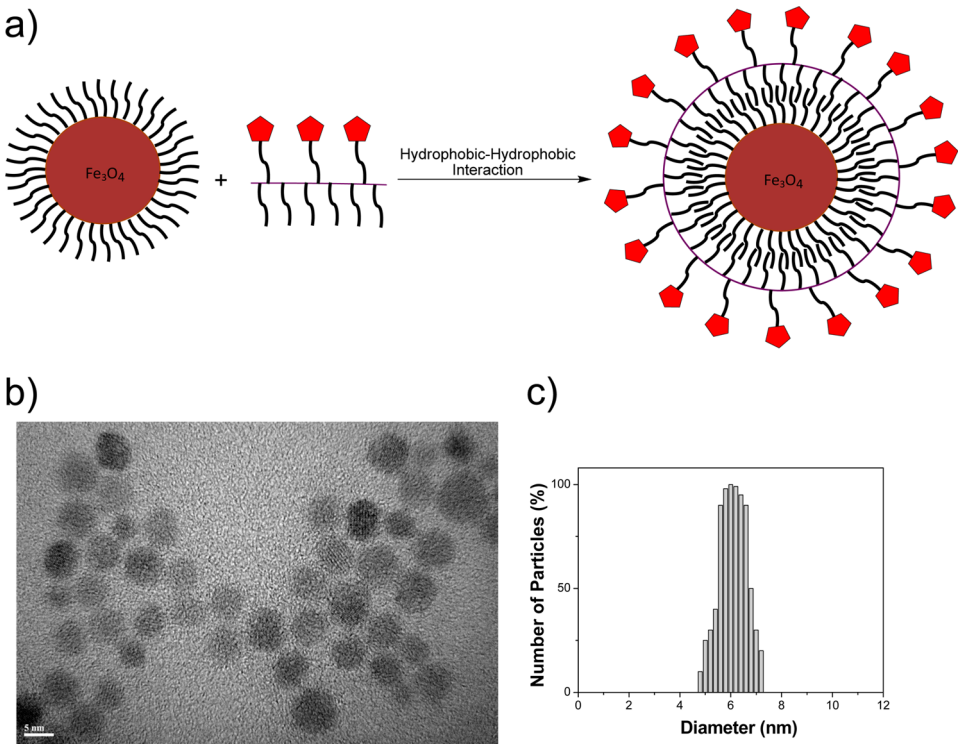

Figure 1. (a) Schematic illustration of Dye-Pol-conjugated Fe_3O_4 magnetic nanoparticles (MNPs) through hydrophobic interaction, yielding MNP@Dye-Pol. (b) HRTEM and (c) size-distribution of MNP@Dye-Pol.

The Dye-Pol conjugate was obtained as a purple-blue powder and characterized by ^{1}H NMR spectroscopy. The polymer Dye-Pol consisted of the following repeating units: functional NIR dye 40%, carboxylic 47%, and *n*-octylamide 13%. As a result, an amphiphilic polymer bearing an organic infrared chromophore for imaging applications and *n*-octylamide side chains, designed for interaction with hydrophobic particles, was obtained. The remaining carboxylic groups, formed during hydrolytic opening of the anhydride ring, and sulfonate groups of NIR fluorescent dye moieties are responsible for the hydrophilic character of the amphiphile and colloidal stability of the particle/polymer assembly.

The zeta potential measurements showed that MNP@Dye-Pol samples were negatively charged, with an electric potential of -31.8 ± 1.2 mV. As a result, MNP@Dye-Pol exhibited good colloidal stability, with no visible aggregation upon 6 months of storage. A high-resolution transmission electron microscopy (HRTEM) image of MNP@Dye-Pol (Figure 1b) shows that the core MNPs with an average diameter of 6.2 ± 0.3 nm (histogram in Figure 1c) are clearly separated from each other. The interparticle distance is *ca.* 1−2 nm, indicating that the Dye-Pol is rather uniformly distributed on the surface of MNPs.

The characteristic absorption spectra of IR-820, IR-820 dye-NH_2, Dye-Pol, and MNP@Dye-Pol are shown in Figure 2A. The maximum absorbance is observed at 820 nm for the first two samples in methanol, whereas the samples, Dye-Pol in MeOH and MNP@Dye-Pol in water, showed maximum absorbance at 656 nm (164 nm blue-shift) and a lower absorption peak at 850 nm. This may be due to the interactions of dye molecules attached to the polymeric backbone through plane-to-plane stacking or head-to-tail arrangement, which is strongly dependent on the nature and length of the linker with the functional group on the amino-NIR cyanine dye or the polymer structure with the NIR cyanine dye conjugates.[35,56]

NIR photoluminescence (PL) spectra of MNP@Dye-Pol and their intermediates were investigated. Figure 2B shows the emission spectra in the NIR region (800−1400 nm), excited at 785 nm. The major emission peak at 1076 nm for control IR-820 dye in methanol blue-shifts for all samples, with a drastic shift to 864 nm for MNP@Dye-Pol in water. However, the Stokes shift of MNP@Dye-Pol in water remained over 200 nm. Dye-Pol and MNP@Dye-Pol showed the emission peaks at 954 and 864 nm, respectively. Interestingly, Dye-Pol and MNP@Dye-Pol displayed a large Stokes shift of ∼298 and 208 nm, respectively (by comparing the more intense absorption peak at 656 nm). The differences in absorption and emission characteristics are presumably due to the electronic state alteration in the dye molecules. There are three specific features in the absorption and emission spectra of these functionalized dyes and conjugated polymer dyes with MNPs. They display (i) a large Stokes shift, (ii) broad emission spectra, and (iii) no mirror image relationship between

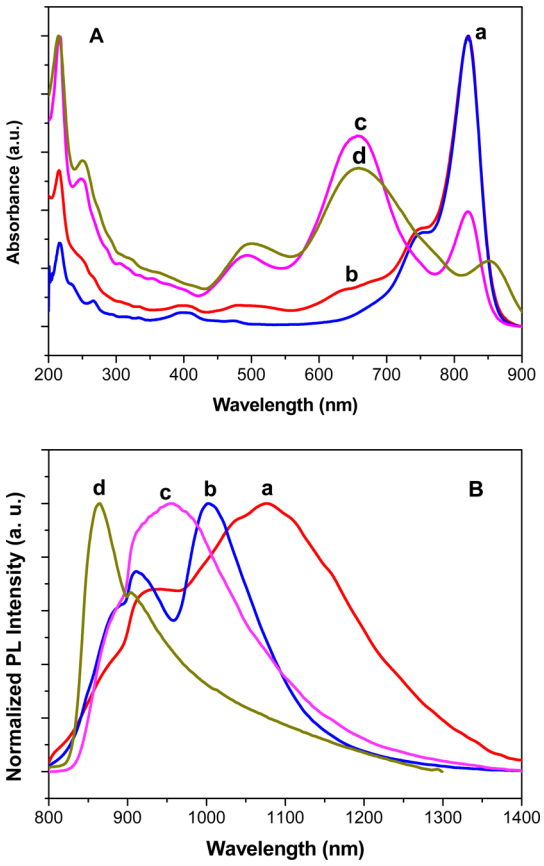

Figure 2. (A) UV−vis−NIR absorption spectra of (a) IR-820, (b) IR-820 dye-NH_2, (c) Dye-Pol in MeOH (0.1 mM, 25 °C), and (d) MNP@Dye-Pol in DI water. (B) NIR photoluminescence spectra of (a) IR-820, (b) IR-820 dye-NH_2, (c) Dye-Pol, and (d) MNP@Dye-Pol, excited with a 785 nm laser diode.

the absorption and emission spectra. The intramolecular charge transfer[34,57] or excited-state proton transfer may play a role in these features.[33,58]

In the literature it has been shown that the absorbance of IR-820 (modified with PEG groups) depends on the solvent. In methanol, IR-820 showed an absorption peak at 820 nm, whereas in water it occurred at 691 nm. It was also observed that the emission of IR-820 in water did not depend on the excitation wavelengths at 785 and 691 nm.[59] In another interesting work, the spectra for free IR-820 revealed excitation and emission peaks at 710 and 820 nm (Stokes shift of 110 nm), respectively.[60] Our unmodified dye showed a Stokes shift of 106 nm (while comparing the absorbance at 820 nm and first emission peak at 926 nm), which is comparable to the above literature.

NIR Labeling and Cytotoxicity. In order to demonstrate the potential of bimodal probes in NIR fluorescence-based biolabeling application, we examined the cellular uptake of MNP@Dye-Pol by HeLa cells. Figure 3a shows an array of labeled cells with DAPI (blue), NIR particles (red), gray, and overlaid images of internalized particles after 2 h of incubation. Control cells are also shown for comparison. It is clear that the NIR particles labeled the whole cell and more fluorescence intensity is seen near the perinuclear region, indicating that the cells are taking part in normal physiological functions in the presence of foreign NPs. The nuclear signal corresponding to healthy cells suggests that the NIR NPs could be used for cellular targeting without any particle-induced cell death signal.

In normal physiology, the cell senses the surrounding material and uses various mechanisms for cellular uptake. It has been shown earlier that superparamagnetic iron oxide NPs with different surface coatings can differentially affect signal transduction pathways.[61] The cell responses to the same amounts of NPs have been found to be significantly dependent on the cell types. The effects of cell vision play a dominant role in the physicochemical effects of MNPs in assessing the toxicity.[62] The functionalized NPs can be internalized, by nonspecific endocytosis, within the first hour and localized mainly in the endosomes or accumulated in the perinuclear region within the cells. This is in good agreement with the findings of most of the NPs discussed in the review.[63]

To evaluate the cytotoxicity of the newly fabricated polymer/particle assemblies, tests were carried out on HeLa cells in the presence of MNP@Dye-Pol at different concentrations (0.1−0.0001 mg/mL). Figure 3b shows the viability of cells that were incubated with MNP@Dye-Pol for 24 h. It was observed that MNP@Dye-Pol displayed a lower toxicity (*ca.* 90% viability) to HeLa cells at the highest concentration tested (0.1 mg/mL). For the second assay, the cells were incubated with MNP@Dye-Pol for 6 h. The second assay looked at how the cells proliferated over time after brief exposure to the particles. Also at 6 h incubation, MNP@Dye-Pol exhibited a lower toxicity (*ca.* 95% viability) at the highest concentration (0.1 mg/mL).

After endocytosis of MNP@Dye-Pol particles, the cells proliferate faster after 6 h of incubation in comparison with those cells with particles after 24 h of incubation (Figure 3b). In the literature, mostly, all types of NPs enter into cells *via* endocytosis pathways and accumulate within intracellular vesicles.[63] It has also been shown earlier that the lysosomal and mitochondrial protein activities correlate to either low or high energy demand for the endocytotic pathways, resulting in an increase or decrease in proliferation, respectively.[64] In accordance with previous literature, we believe that during the early stages of exposure (6 h) of MNP@Dye-Pol particles, the low-energy consumption might induce an increase in cell cycle, proliferation rate, and cell viability.

The iron oxide MNPs are known to accelerate spin−spin relaxation rate (T_2^{-1} or R_2) of water protons and exert negative contrast in MRI. Figure 4A shows the T_2-weighted MR images of MNP@Dye-Pol. Samples of

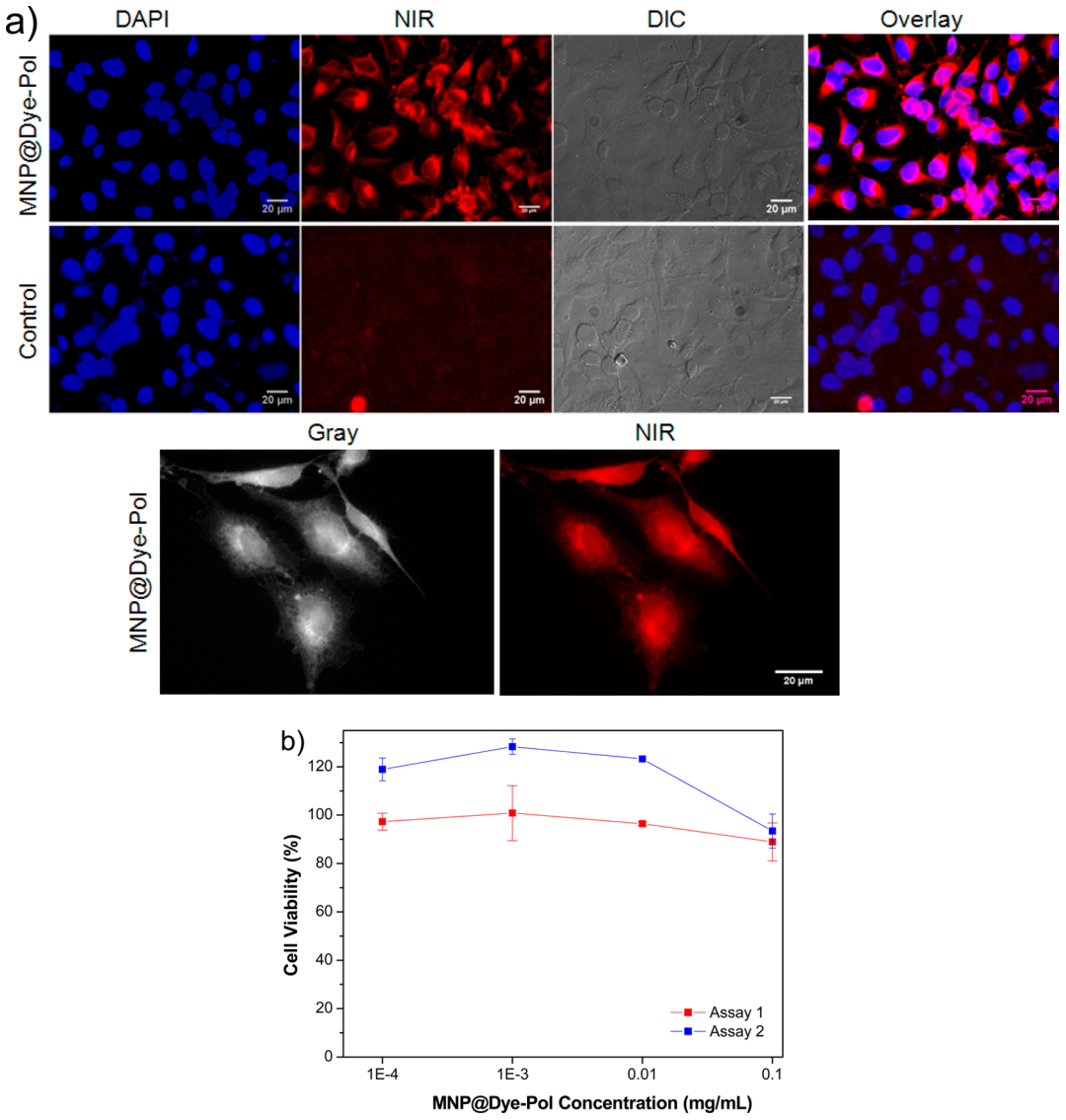

Figure 3. (a) Labeling of HeLa cells incubated for 2 h with 50 μL of MNP@Dye-Pol (1 mg/mL). Blue (DAPI), red (NIR), and DIC channels. (Lower panel) Images at high magnification. Scale bar: 20 μm. (b) *In vitro* cell viability of HeLa cells incubated for 24 h (assay 1) and 6 h (assay 2) at 37 °C with different concentrations of MNP@Dye-Pol. Cell viability assays were carried out using CellTiter-Blue in triplicate. The error bars represent the standard deviations.

MNP@Dye-Pol were prepared in the concentration range 0.015−0.75 mM. The relaxation rate is enhanced as the concentration of the particles increases, resulting in a negative T_2 contrast. The specific relaxivity (r_2) evaluated from a plot of the relaxation rate (T_2^{-1}) *versus* the NP concentration was estimated to be 4.41 mM^{-1} s^{-1} for MNP@Dye-Pol (Figure 4B). In order to demonstrate the application of the newly synthesized MNP@Dye-Pol as bimodal probes, *in vivo* animal imaging was carried out in a murine model on a 7T MRI system. In Figure 4C, sites a and b represent two samples of MNP@Dye-Pol (derived from low and high molecular weight polymer; M_w 6000 and 60 000, respectively) fixed in 0.8% agarose. It is clear from the image (site a) that the MNP@Dye-Pol generated a good negative T_2 contrast. These preliminary data demonstrated that our particles can be further used for targeted *in vivo* application, which will be the focus of our future studies.

CONCLUSION

We have demonstrated a reproducible synthesis of novel water-soluble, bimodal MNP@Dye-Pol probes for optical and MR imaging. The excellent water solubility and photochemical properties have been preserved after the chemical modification of dyes and functionalization with polymers. We have established a simple and versatile approach for the synthesis of IR-820 dye-NH_2 *via* a one-step synthetic pathway without a catalyst, resulting in high purity and yield. Furthermore, MR animal and NIR cellular imaging studies together with cytotoxicity assays have demonstrated clearly that these less toxic bimodal probes have great potential in optical and

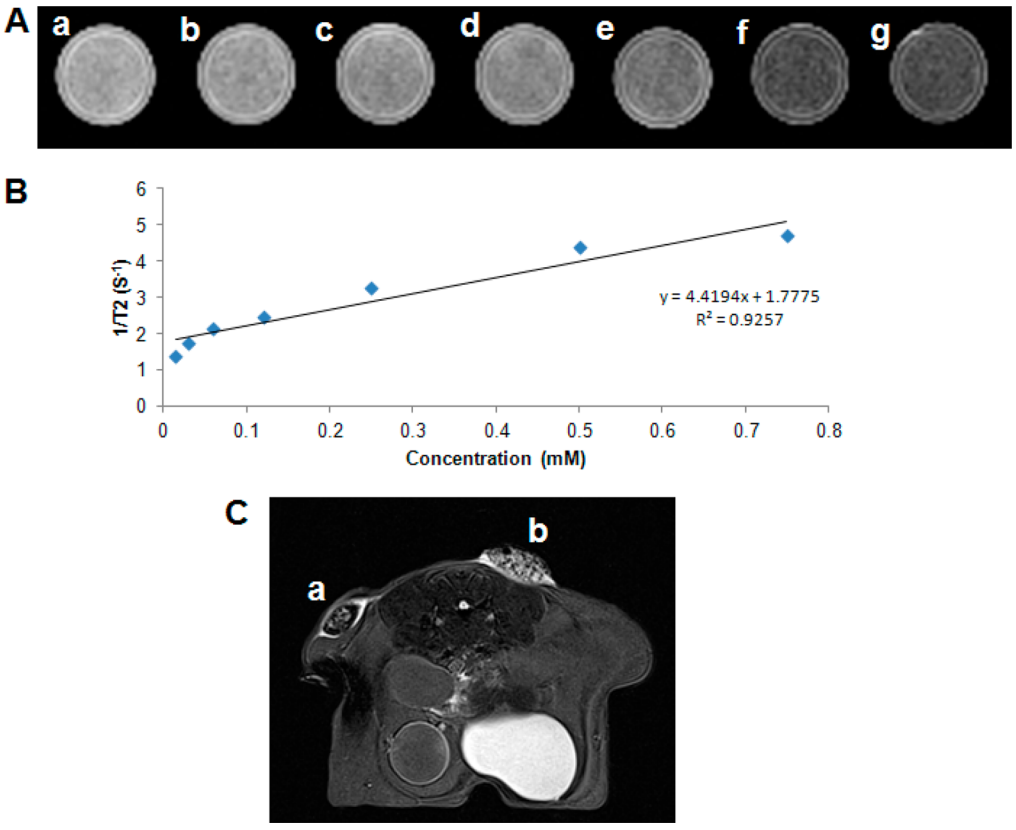

Figure 4. T_2 phantom images, relaxivity data, and *in vivo* MR imaging. (A) T_2-weighted images at different concentrations of MNP@Dye-Pol: (a) 0.015, (b) 0.03, (c) 0.06, (d) 0.12, (e) 0.25, (f) 0.5, (g) 0.75 mM. (B) Relaxivity curve of MNP@Dye-Pol. The magnetic field and temperature were 300 MHz (7 Tesla) and 27 °C, respectively. (C) T_2-weighted MR imaging of a murine model after subcutaneous injection of 0.7 mM MNP@Dye-Pol fixed in 0.8% agarose. Site a is the MNP@Dye-Pol (derived from low molecular weight polymer; M_w 6000), and site b is the MNP@Dye-Pol (derived from high molecular weight polymer; M_w 60 000).

MR imaging applications. We believe this study would enhance the limited market value of FDA-approved NIR fluorescent dyes in life science, opening up new avenues in the area of multimodal imaging.

METHODS

Materials. IR-820, ethylenediamine, BuLi in 2.5 M hexane, poly(isobutylene-*alt*-maleic anhyride), *n*-octylamine, and *N,N*-diisopropylethylamine (DIPEA), silica gel, sodium hydroxide, and solvents including anhydrous DMF, anhydrous THF, dichloromethane, and ethanol were purchased from Sigma-Aldrich and used as received. Phosphate-buffered saline (PBS, PAA H15-002) was stored at room temperature. All the tissue culture reagents were obtained from Invitrogen (Singapore). Dulbecco's modified Eagle's medium (DMEM, Invitrogen 11965), CellTiter-Blue (Promega G8081), 10% fetal bovine serum (FBS), penicillin, and streptomycin were stored at 4 °C.

Synthesis. All operations were performed in the Schlenk line and the glovebox. Core iron oxide (Fe_3O_4) MNPs were synthesized according to the literature method.[55]

Synthesis of IR-820 Dye-NH_2. IR-820 (0.5 g, 0.58 mmol) was dried under vacuum for 15 min and subsequently purged with argon for another 15 min in a Schlenk line. Anhydrous DMF (2 mL) was added, and the mixture was stirred at room temperature for 30 min. A mixture of ethylenediamine (3.6 g, 59.8 mmol) and BuLi (0.8 mL, 2 mmol) in 2.5 M hexane was prepared in a glovebox and added dropwise to the reaction flask at −30 °C. The mixture was warmed to room temperature and stirred overnight. The red solution thus obtained was pump dried. The crude product was purified by column chromatography on silica gel (dichloromethane/ethanol, 6:4), and a glossy green solid obtained. Yield: 0.463 g (0.53 mmol, 91%).

Synthesis of Dye-Pol. A mixture of poly(isobutylene-*alt*-maleic anhyride) (0.099 g) (M_w = 6000 g/mol), *n*-octylamine (0.2 mL, 0.15 mmol), and DIPEA (1 mL) was suspended in anhydrous THF (20 mL) and stirred for 30 min at room temperature. The dye (0.463 g, 0.53 mmol) dissolved in 20 mL of THF and 2 mL of DMF was added to the polymer mixture, and stirring continued at room temperature overnight. After the evaporation of THF, the mixture was suspended in water and a small excess of NaOH added with respect to the amount of carboxylic groups in the polymer backbone. The obtained mixture was dialyzed against a 0.01 M solution of NaOH for one day and against pure water for several days (membrane cutoff 6000D). The dialyzed water solution was freeze-dried. Yield: 0.10 g.

Synthesis and Purification of MNP@Dye-Pol. To 5 mg of Dye-Pol suspended in THF (10 mL) was added 5 mg of MNPs in 7 mL of deionized water in a one-neck round-bottom flask. The mixture was concentrated in a rotary evaporator to 6−8 mL volume by removing THF and water. This method was modified from the literature.[52−54] Nanoparticle−polymer assemblies (MNP@Dye-Pol) were purified by gentle, slow centrifugation to remove excess free polymer. This process was rather efficient, and the concentration of the solution was 1 mg/mL. Some residual amount of polymer may be present in the solution. However, due to multiple hydrophobic attachments, this method can produce a stable polymer shell.

Structural Characterization. ^{1}H and ^{13}C NMR spectra were recorded on a Bruker DRX 400 MHz spectrometer equipped with a broadband observe probe. MALDI-TOF mass spectra were obtained using an Autoflex II TOF/TOF system from Bruker Daltonics. UV−vis absorption spectra were taken on a UV-3600 Shimadzu UV−vis−NIR spectrophotometer, and NIR photoluminescence spectra were measured using a JY LabRAM HR system. The colloidal stability results were obtained by using the Brookhaven Instruments ZetaPlus zeta potential analyzer. TEM images were acquired with a JEOL TEM-2100 transmission electron microscope. FTIR spectra were recorded using a Fourier transform infrared spectrometer, FTIR PerkinElmer.

NIR Labeling. HeLa cells were obtained from ATCC (Manassas, VA, USA) and grown in 75 cm^2 tissue culture flask up to 80% confluence in DMEM containing 10% FBS and 1% antibiotics (penicillin and streptomycin). For labeling experiments, cells were split into a six-well tissue culture plate containing an 18 × 18 mm prewashed and sterilized cover glass at 1.5 × 10^5 cells/well for 24 h before incubating with MNP@Dye-Pol NPs. Each well is loaded with 20 μL of NPs (1 mg/mL concentration) in 1.0 mL of culture media and incubated for 2 h. Cells were further washed with 1× PBS three times and fixed using 4% paraformaldehyde (Sigma) followed by PBS washing. The fixed cells were mounted on cover slides using Hydromount (National Diagnostic) and used for imaging.

The fluorescence imaging of cells was obtained using an upright AxioImager Z1 (Zeiss) microscope equipped with a Photometrics coolSNAPHQ camera by selecting a 63X/1.4 plan apochromatT objective lens. The excitation and emission were performed using 769/41 nm BrightLine single-bandpass and 830 nm RazorEdge ultrasteep long-pass edge filters, respectively, with an 801 nm edge BrightLine single-edge (Semrock) dichroic mirror. The images were further processed using Fiji ImageJ software.

Cell Culture and Cell Viability Assays. HeLa human cervix adenocarcinoma cells were grown in DMEM supplemented with 10% fetal bovine serum, 100 units/mL penicillin, and 100 μg/mL streptomycin and cultured in a 5% CO_2 humidified atmosphere at 37 °C. 10^4 HeLa cells per well were seeded in a 96-well plate. Following incubation overnight, cell culture medium was removed and 100 μL of MNP samples diluted in serum-free DMEM was added to the cells. The MNP@Dye-Pol samples were then removed after 6 h of incubation at 37 °C, and the treated cells were washed with PBS. Complete DMEM was added, and the cells were cultured for another 48 h. Thereafter, 20 μL of CellTiter-Blue was added to the cells. After incubation at 37 °C for 3 h, the fluorescence was measured at 595 nm with excitation at 560 nm using a Tecan Infinite 200 microplate reader. The results were expressed in percentage based on the control with untreated cells. For the 24 h incubation experiment, 2 × 10^4 cells per well were seeded in a 96-well plate. Following incubation overnight, culture medium was removed and 100 μL of MNP samples in serum-free DMEM was added to the cells for 24 h. Subsequently, the cell viability assay was carried out as described above. All experiments were performed in triplicates.

***In Vivo* MRI.** T_2-weighted MR images were acquired with a 7T MRI system (Bruker, ClinScan). The imaging of a mouse was performed under the following conditions. One nude (nu/nu, Balb/c) mouse was anesthetized by inhalation of isoflurane. The body temperature was maintained at 38 ± 1 °C. The spin echo sequence was optimized to generate T_2-weighted images. The MNP@Dye-Pol NPs of about 200 μL were fixed in agarose and subcutaneously injected in the flank region of the mouse. The T_2-weighted images were acquired with the following acquisition parameters: repetition time (TR) and echo time (TE), TR/TE = 1590/74 ms, with 8 averages and field of view (FOV) = 40 mm.

Conflict of Interest: The authors declare no competing financial interest.

Acknowledgment. The authors thank C. B. Koh, Y. C. J. Tan, and H. R. Tan at the IMRE for their technical support. Q. Dou and S. Dalapati are acknowledged for their help with emission measurements. This work is funded by the Agency for Science, Technology and Research (A*STAR) Joint Council Office (JCO) Grant JCOAG03_FG03_2009, Singapore.

Supporting Information Available: Characterization of IR-820 dye-NH_2 by ^{1}H and ^{13}C NMR spectra and Dye-Pol by ^{1}H NMR. This material is available free of charge *via* the Internet at http://pubs.acs.org.

REFERENCES AND NOTES

1. Gao, J.; Gu, H.; Xu, B. Multifunctional Magnetic Nanoparticles: Design, Synthesis and Biomedical Applications. *Acc. Chem. Res.* **2009**, *42*, 1097–1107.
2. Mahmoudi, M.; Serpooshan, V. Silver-Coated Engineered Magnetic Nanoparticles Are Promising for the Success in the Fight against Antibacterial Resistance Threat. *ACS Nano* **2012**, *6*, 2656–2664.
3. Jin, Y.; Jia, C.; Huang, S. W.; O'Donnell, M.; Gao, X. Multifunctional Nanoparticles as Coupled Contrast Agents. *Nat. Commun.* **2010**, *1*, 1–8.
4. Laurent, S.; Forge, D.; Port, M.; Roch, A.; Robic, C.; Elst, L. V.; Muller, R. N. Magnetic Iron Oxide Nanoparticles: Synthesis, Stabilization, Vectorization, Physicochemical Characterizations, and Biological Applications. *Chem. Rev.* **2008**, *108*, 2064–2110.
5. Alcantara, D.; Guo, Y.; Yuan, H.; Goergen, C. J.; Chen, H. H.; Cho, H.; Sosnovik, D. E.; Josephson, L. Fluorochrome-Functionalized Magnetic Nanoparticles for High-Sensitivity Monitoring of the Polymerase Chain Reaction by Magnetic Resonance. *Angew. Chem., Int. Ed.* **2012**, *51*, 6904–6907.
6. Xie, J.; Liu, G.; Eden, H. S.; Ai, H.; Chen, X. Surface-Engineered Magnetic Nanoparticle Platforms for Cancer Imaging and Therapy. *Acc. Chem. Res.* **2011**, *44*, 883–892.
7. Tassa, C.; Shaw, S. Y.; Weissleder, R. Dextran-Coated Iron Oxide Nanoparticles: A Versatile Platform for Targeted Molecular Imaging, Molecular Diagnostics, and Therapy. *Acc. Chem. Res.* **2011**, *44*, 842–852.
8. Gao, J.; Zhang, W.; Huang, P.; Zhang, B.; Zhang, X.; Xu, B. Intracellular Spatial Control of Fluorescent Magnetic Nanoparticles. *J. Am. Chem. Soc.* **2008**, *130*, 3710–3711.
9. Ang, C. Y.; Giam, L.; Chan, Z. M.; Lin, A. W. H.; Gu, H.; Devlin, E.; Papaefthymiou, G. C.; Selvan, S. T.; Ying, J. Y. Facile Synthesis of Fe_2O_3 Nanocrystals without $Fe(CO)_5$ Precursor and One-Pot Synthesis of Highly Fluorescent Fe_2O_3-CdSe Nanocomposites. *Adv. Mater.* **2009**, *21*, 869–873.
10. Selvan, S. T.; Patra, P. K.; Ang, C. Y.; Ying, J. Y. Synthesis of Silica-Coated Semiconductor and Magnetic Quantum Dots and Their Use in the Imaging of Live Cells. *Angew. Chem., Int. Ed.* **2007**, *46*, 2248–2452.
11. Zhu, Z.-J.; Yeh, Y.-C.; Tang, R.; Yan, B.; Tamayo, J.; Vachet, R. W.; Rotello, V. M. Stability of Quantum Dots in Live Cells. *Nat. Chem.* **2011**, *3*, 963–968.
12. Smith, A. M.; Duan, H.; Mohs, A. M.; Nie, S. Bioconjugated Quantum Dots for *in Vivo* Molecular and Cellular Imaging. *Adv. Drug Delivery Rev.* **2008**, *60*, 1226–1240.
13. Mishra, A.; Behera, R. K.; Behera, P. K.; Mishra, B. K.; Behera, G. B. Cyanines during the 1990s: A Review. *Chem. Rev.* **2000**, *100*, 1973–2011.
14. Frangioni, J. V. *In Vivo* Near-Infrared Fluorescence Imaging. *Curr. Opin. Chem. Biol.* **2003**, *7*, 626–634.
15. Xiong, L.; Shuhendler, A. J.; Rao, J. Self-Luminescing BRET-FRET Near-Infrared Dots for *in Vivo* Lymph-Node Mapping and Tumour Imaging. *Nat. Commun.* **2012**, 10.1038/ncomms2197.
16. Baumes, J. M.; Gassensmith, J. J.; Giblin, J.; Lee, J.-J.; White, A. G.; Culligan, W. J.; Leevy, W. M.; Kuno, M.; Smith, B. D. Storable, Thermally Activated, Near-Infrared Chemiluminescent Dyes and Dye-Stained Microparticles for Optical Imaging. *Nat. Chem.* **2010**, *2*, 1025–1030.
17. Weissleder, R. *In Vivo* Imaging of Tumors with Protease-Activated Near-Infrared Fluorescent Probes. *Nat. Biotechnol.* **1999**, *17*, 375–378.
18. Becker, A.; Hessenius, C.; Licha, K.; Ebert, B.; Sukowski, U.; Semmler, W.; Wiedenmann, B.; Grötzinger, C. Receptor-Targeted Optical Imaging of Tumors with Near-Infrared Fluorescent Ligands. *Nat. Biotechnol.* **2001**, *19*, 327–331.

19. Hilderbrand, S. A.; Kelly, A.; Weissleder, R.; Tung, C. H. Monofunctional Near-Infrared Fluorochromes for Imaging Application. *Bioconjugate Chem.* **2005**, *16*, 1275–1281.
20. Cheng, Z.; Levi, J.; Xiong, Z.; Gheysens, O.; Keren, S.; Chen, X.; Gambhir, S. S. Near-Infrared Fluorescent Deoxyglucose Analogue for Tumor Optical Imaging in Cell Culture and Living Mice. *Bioconjugate Chem.* **2006**, *17*, 662–669.
21. Kim, S.; Lim, Y. T.; Soltesz, E. G.; Grand, A. M. D.; Lee, J.; Nakayama, A.; Parker, J. A.; Mihaljevic, T.; Laurence, R. G.; Dor, D. M.; *et al*. Near-Infrared Fluorescent Type II Quantum Dots for Sentinel Lymph Node Mapping. *Nat. Biotechnol.* **2004**, *22*, 93–97.
22. Sasaki, E.; Kojima, H.; Nishimatsu, H.; Urano, Y.; Kikuchi, K.; Hirata, Y.; Nagano, T. Highly Sensitive Near-Infrared Fluorescent Probes for Nitric Oxide and their Application to Isolated Organs. *J. Am. Chem. Soc.* **2005**, *127*, 3684–3685.
23. Tang, B.; Huang, H.; Xu, K.; Tong, L.; Yang, G.; Liu, X.; An, L. Highly Sensitive and Selective Near-Infrared Fluorescent Probe for Zinc and its Application to Macrophage Cells. *Chem. Commun.* **2006**, 3609–3611.
24. Kiyose, K.; Kojima, H.; Urano, Y.; Nagano, T. Development of a Ratiometric Fluorescent Zinc Ion Probe in Near-Infrared Region, Based on Tricarbocyanine Chromophore. *J. Am. Chem. Soc.* **2006**, *128*, 6548–6549.
25. Tang, B.; Cui, L. J.; Xu, K. H.; Tong, L. L.; Yang, G. W.; An, L. G. A Sensitive and Selective Near-Infrared Fluorescent Probe for Mercuric Ions and its Biological Imaging Applications. *ChemBioChem* **2008**, *9*, 1159–1164.
26. Weissleder, R.; Ntziachristos, V. Shedding Light onto Live Molecular Targets. *Nat. Med.* **2003**, *9*, 123–128.
27. Zaheer, A.; Lenkinski, R. E.; Mahmood, A.; Jones, A. G.; Cantley, L. C.; Frangioni, J. V. *In Vivo* Near-Infrared Fluorescence Imaging of Osteoblastic Activity. *Nat. Biotechnol.* **2001**, *19*, 1148–1154.
28. Zhang, Z.; Achilefu, S. Synthesis and Evaluation of Polyhydroxylated Near-Infrared Carbocyanine Molecular Probes. *Org. Lett.* **2004**, *6*, 2067–2070.
29. Strekowski, L.; Lipowska, M.; Patonay, G. Substitution Reactions of a Nucleofugal Group in Heptamethine Cyanine Dyes. Synthesis of an Isothiocyanato Derivative for Labeling of Proteins with a Near-Infrared Chromophore. *J. Org. Chem.* **1992**, *57*, 4578–4580.
30. Gallaher, D. L.; Johnson, M. E. Development of Near-Infrared Fluorophoric Labels for the Determination of Fatty Acids Separated by Capillary Electrophoresis with Diode Laser Induced Fluorescence Detection. *Analyst* **1999**, *124*, 1541–1546.
31. Narayanan, N.; Patonay, G. A New Method for the Sythesis of Heptamethine Cyanine Dyes: Synthesis of New Near-Infrared Fluorescent Labels. *J. Org. Chem.* **1995**, *60*, 2391–2395.
32. Lee, H.; Mason, J. C.; Achilefu, S. Synthesis and Spectral Properties of Near-Infrared Aminophenyl, Hydroxyphenyl-, and Phenyl-Substituted Heptamethine Cyanines. *J. Org. Chem.* **2008**, *73*, 723–725.
33. Kiyose, K.; Aizawa, S.; Sasaki, E.; Kojima, H.; Hanaoka, K.; Terai, T.; Urano, Y.; Nagano, T. Molecular Design Strategies for Near-Infrared Ratiometric Fluorescent Probes Based on the Unique Spectral Properties of Aminocyanines. *Chem.—Eur. J.* **2009**, *15*, 9191–9200.
34. Peng, X.; Song, F.; Lu, E.; Wang, Y.; Zhou, W.; Fan, J.; Gao, Y. Heptamethine Cyanine Dyes with a Large Stokes Shift and Strong Fluorescence: A Paradigm for Excited-State Intramolecular Charge Transfer. *J. Am. Chem. Soc.* **2005**, *127*, 4170–4171.
35. Ornelas, C.; Lodescar, R.; Durandin, A.; Canary, J. W.; Pennell, R.; Liebes, L. F.; Weck, M. Combining Aminocyanine Dyes with Polyamide Dendrons: A Promising Strategy for Imaging in the Near-Infrared Region. *Chem.—Eur. J.* **2011**, *17*, 3619–3629.
36. Masotti, A.; Vicennati, P.; Boschi, F.; Calderan, L.; Sbarbati, A.; Ortaggi, G. A Novel Near-Infrared Indocyanine Dye-Polyethylenimine Conjugate Allows DNA Delivery Imaging *in Vivo*. *Bioconjugate Chem.* **2008**, *19*, 983–987.
37. Masotti, A.; Moretti, F.; Mancini, F.; Russo, G.; Lauro, N. D.; Checchia, P.; Marianecci, C.; Carafa, M.; Santucci, E.; Ortaggi, G. Physicochemical and Biological Study of Selected Hydrophobic Polyethylenimine-Based Polycationic Liposomes and Their Complexes with DNA. *Bioorg. Med. Chem.* **2007**, *15*, 1504–1515.
38. Josephson, L.; Kircher, M. F.; Mahmood, U.; Tang, Y.; Weissleder, R. Near-Infrared Fluorescent Nanoparticles as Combined MR/Optical Imaging Probes. *Bioconjugate Chem.* **2002**, *13*, 554–560.
39. Kircher, M. F.; Mahmood, U.; King, R. S.; Weissleder, R.; Josephson, L. A Multimodal Nanoparticle for Preoperative Magnetic Resonance Imaging and Intraoperative Optical Brain Tumor Delineation. *Cancer Res.* **2003**, *63*, 8122–8125.
40. Moore, A.; Medarova, Z.; Potthast, A.; Dai, G. *In Vivo* Targeting of Underglycosylated MUC-1 Tumor Antigen Using a Multimodal Imaging Probe. *Cancer Res.* **2004**, *64*, 1821–1827.
41. Schellenberger, E. A.; Sosnovik, D.; Weissleder, R.; Josephson, L. Magneto/Optical Annexin V, a Multimodal Protein. *Bioconjugate Chem.* **2004**, *15*, 1062–1067.
42. Kelly, K. A.; Allport, J. R.; Tsourkas, A.; Shinde-Patil, V. R.; Josephson, L.; Weissleder, R. Detection of Vascular Adhesion Molecule-1 Expression Using a Novel Multimodal Nanoparticle. *Circ. Res.* **2005**, *96*, 327–336.
43. Veiseh, O.; Sun, C.; Gunn, J.; Kohler, N.; Gabikian, P.; Lee, D.; Bhattarai, N.; Ellenbogen, R.; Sze, R.; Hallahan, A.; Olson, J.; Zhang, M. Optical and MRI Multifunctional Nanoprobe for Targeting Gliomas. *Nano Lett.* **2005**, *5*, 1003–1008.
44. Sosnovik, D. E.; Schellenberger, E. A.; Nahrendorf, M.; Novikov, M. S.; Matsui, T.; Dai, G.; Reynolds, F.; Grazette, L.; Rosenzweig, A.; Weissleder, R.; *et al*. Magnetic Resonance Imaging of Cardiomyocyte Apoptosis with a Novel Magneto-Optical Nanoparticle. *Magn. Reson. Med.* **2005**, *54*, 718–724.
45. Montet, X.; Montet-Abou, K.; Reynolds, F.; Weissleder, R.; Josephson, L. Nanoparticle Imaging of Integrins on Tumor Cells. *Neoplasia* **2006**, *8*, 214–222.
46. Tréhin, R.; Figueiredo, J.-L.; Pittet, M. J.; Weissleder, R.; Josephson, L.; Mahmood, U. Fluorescent Nanoparticle Uptake for Brain Tumor Visualization. *Neoplasia* **2006**, *8*, 302–311.
47. Lee, C.-M.; Jang, D. R.; Kim, J.; Cheong, S.-J.; Kim, E.-M.; Jeong, M.-H.; Kim, S.-H.; Kim, D. W.; Lim, S. T.; Sohn, M.-H.; *et al*. Oleyl-Chitosan Nanoparticles Based on a Dual Probe for Optical/MR Imaging *in Vivo*. *Bioconjugate Chem.* **2011**, *22*, 186–192.
48. Sun, C.; Du, K.; Fang, C.; Bhattarai, N.; Veiseh, O.; Kievit, F.; Stephen, Z.; Lee, D.; Ellenbogen, R. G.; Ratner, B.; Zhang, M. PEG-Mediated Synthesis of Highly Dispersive Multifunctional Superparamagnetic Nanoparticles: Their Physicochemical Properties and Function *in Vivo*. *ACS Nano* **2010**, *4*, 2402–2410.
49. Miwa, N.; Inagaki, M.; Eguchi, H.; Okumura, M.; Inagaki, Y.; Harada, T. Near Infrared Fluorescent Contrast Agent and Fluorescence Imaging. US 7,488,468 B1, 2009.
50. Pellegrino, T.; Manna, L.; Kudera, S.; Liedl, T.; Koktysh, D.; Rogach, A. L.; Keller, S.; Rädler, J.; Natile, G.; Parak, W. J. Hydrophobic Nanocrystals Coated with an Amphiphilic Polymer Shell: A General Route to Water Soluble Nanocrystals. *Nano Lett.* **2004**, *4*, 703–707.
51. Yakovlev, A. V.; Zhang, F.; Zulqurnain, A.; Azhar-Zahoor, A.; Luccardini, C.; Gaillard, S.; Mallet, J.-M.; Tauc, P.; Brochon, J.-C.; Parak, W. J.; *et al*. Wrapping Nanocrystals with an Amphiphilic Polymer Preloaded with Fixed Amounts of Fluorophore Generates FRET-Based Nanoprobes with a Controlled Donor/Acceptor Ratio. *Langmuir* **2009**, *25*, 3232–3239.
52. Jańczewski, D.; Tomczak, N.; Liu, S.; Han, M.-Y.; Vansco, G. J. Covalent Assembly of Functional Inorganic Nanoparticles by "Click" Chemistry in Water. *Chem. Commun.* **2010**, *46*, 3253–3255.
53. Jańczewski, D.; Tomczak, N.; Han, M.-Y.; Vansco, G. J. Synthesis of Functionalized Amphiphilic Polymers for Coating Quantum Dots. *Nat. Protoc.* **2011**, *6*, 1546–1553.
54. Jańczewski, D.; Tomczak, N.; Khin, Y. W.; Han, M.-Y.; Vancso, G. J. Designer Multi-Functional Comb-Polymers for Surface

Engineering of Quantum Dots on the Nanoscale. *Eur. Polym. J.* **2009**, *45*, 3–9.
55. Xu, Z.; Shen, C.; Hou, Y.; Gao, H.; Sun, S. Oleylamine as Both Reducing Agent and Stabilizer in a Facile Synthesis of Magnetite Nanoparticles. *Chem. Mater.* **2009**, *21*, 1778–1780.
56. Eisele, D. M.; Cone, C. W.; Bloemsma, E. A.; Vlaming, S. M.; van der Kwaak, C. G. F.; Silbey, R. J.; Bawendi, M. G.; Knoester, J.; Rabe, J. P.; Vanden Bout, D. A. Utilizing Redox-Chemistry to Elucidate the Nature of Exciton Transitions in Supramolecular Dye Nanotubes. *Nat. Chem.* **2012**, *4*, 655–662.
57. Benniston, A. C.; Harriman, A.; Lawrie, D. J.; Mayeux, A. The Photophysical Properties of a Pyrene-Thiophene-Terpyridine Conjugate and of Its Zinc(II) and Ruthenium(II) Complexes. *Phys. Chem. Chem. Phys.* **2004**, *6*, 51–57.
58. Kaneda, K.; Arai, T. Photoinduced Hydrogen Atom Transfer in *trans*-1-(1′-Hydroxy-2′-naphthyl)-3-(1-naphthyl)-2-propen-1-one. *Photochem. Photobiol. Sci.* **2003**, *2*, 402–406.
59. Fernandez-Fernandez, A. IR820 Nanoconjugates for Theranostic Applications. FIU Electronic Theses and Dissertations, 2013, Paper 819. http://digitalcommons.fiu.edu/etd/819.
60. Prajapati, S. I.; Martinez, C. O.; Bahadur, A. N.; Wu, I. Q.; Zheng, W.; Lechleiter, J. D.; McManus, L. M.; Chisholm, G. B.; Michalek, J. E.; Shireman, P. K.; Keller, C. Near-Infrared Imaging of Injured Tissue in Living Subjects Using IR-820. *Mol. Imaging* **2009**, *8*, 45–54.
61. Rauch, J.; Kolch, W.; Mahmoudi, M. Cell Type-Specific Activation of AKT and ERK Signaling Pathways by Small Negatively-Charged Magnetic Nanoparticles. *Sci. Rep.* **2012**, *2*, 86810.1038/srep00868.
62. Mahmoudi, M.; Laurent, S.; Shokrgozar, M. A.; Hosseinkhani, M. Toxicity Evaluations of Superparamagnetic Iron Oxide Nanoparticles: Cell "Vision" *versus* Physicochemical Properties of Nanoparticles. *ACS Nano* **2011**, *5*, 7263–7276.
63. Lewinski, N.; Colvin, V.; Drezek, R. Cytotoxicity of Nanoparticles. *Small* **2008**, *4*, 26–49.
64. Di Virgilio, A. L.; Reigosa, M.; de Mele, M. F. L. Response of UMR 106 Cells Exposed to Titanium Oxide and Aluminum Oxide Nanoparticles. *J. Biomed. Mater. Res. A* **2009**, *92A*, 80–86.